



**HAL**  
open science

## The 15 January 2022 Hunga Tonga Eruption History as Inferred From Ionospheric Observations

E. Astafyeva, B. Maletckii, T. D. Mikesell, E. Munaibari, M. Ravanelli, P. Coisson, F. Manta, Lucie Rolland

► **To cite this version:**

E. Astafyeva, B. Maletckii, T. D. Mikesell, E. Munaibari, M. Ravanelli, et al.. The 15 January 2022 Hunga Tonga Eruption History as Inferred From Ionospheric Observations. *Geophysical Research Letters*, 2022, 49 (10), pp.e2022GL098827. 10.1029/2022GL098827 . insu-03688502

**HAL Id: insu-03688502**

**<https://insu.hal.science/insu-03688502>**

Submitted on 19 Aug 2022

**HAL** is a multi-disciplinary open access archive for the deposit and dissemination of scientific research documents, whether they are published or not. The documents may come from teaching and research institutions in France or abroad, or from public or private research centers.

L'archive ouverte pluridisciplinaire **HAL**, est destinée au dépôt et à la diffusion de documents scientifiques de niveau recherche, publiés ou non, émanant des établissements d'enseignement et de recherche français ou étrangers, des laboratoires publics ou privés.

Copyright

# Geophysical Research Letters®

## RESEARCH LETTER

10.1029/2022GL098827

### Key Points:

- Ionospheric total electron content (TEC) data reveal that the 15 January 2022 Hunga Tonga volcanic eruption involved at least five large explosions between 4 and 5 UT
- From TEC observations, we estimate the onset time to be 04:05:54UT and the main explosion energy release of 9–37 Megatons trinitrotoluene equivalent
- The eruption-driven shock wave caused an unprecedentedly strong and long-lasting depletion in the ionosphere

### Supporting Information:

Supporting Information may be found in the online version of this article.

### Correspondence to:

E. Astafyeva,  
astafyeva@ippg.fr

### Citation:

Astafyeva, E., Maletckii, B., Mikesell, T. D., Munaibari, E., Ravanelli, M., Coisson, P., et al. (2022). The 15 January 2022 Hunga Tonga eruption history as inferred from ionospheric observations. *Geophysical Research Letters*, 49, e2022GL098827. <https://doi.org/10.1029/2022GL098827>

Received 29 MAR 2022

Accepted 5 MAY 2022

### Author Contributions:

**Conceptualization:** E. Astafyeva

**Data curation:** B. Maletckii

**Formal analysis:** E. Astafyeva, B.

Maletckii, T. D. Mikesell, E. Munaibari, M. Ravanelli, P. Coisson, F. Manta, L. Rolland

**Investigation:** E. Astafyeva, B.

Maletckii, T. D. Mikesell, E. Munaibari, M. Ravanelli, P. Coisson, F. Manta, L. Rolland

**Methodology:** E. Astafyeva, B.

Maletckii, T. D. Mikesell, E. Munaibari, L. Rolland

**Software:** B. Maletckii, T. D. Mikesell, E. Munaibari, L. Rolland

**Supervision:** E. Astafyeva, L. Rolland

© 2022. American Geophysical Union.  
All Rights Reserved.

## The 15 January 2022 Hunga Tonga Eruption History as Inferred From Ionospheric Observations

E. Astafyeva<sup>1</sup> , B. Maletckii<sup>1</sup> , T. D. Mikesell<sup>2</sup> , E. Munaibari<sup>3</sup> , M. Ravanelli<sup>1</sup>, P. Coisson<sup>1</sup> , F. Manta<sup>3</sup>, and L. Rolland<sup>3</sup>

<sup>1</sup>Université Paris Cité, Institut de physique du globe de Paris (IPGP), CNRS, Paris, France, <sup>2</sup>Norwegian Geotechnical Institute, Natural Hazards, Oslo, Norway, <sup>3</sup>Université Côte d'Azur, Observatoire de la Côte d'Azur, CNRS, IRD, Géoazur, Valbonne, France

**Abstract** On 15 January 2022, the Hunga Tonga-Hunga Ha'apai submarine volcano erupted violently and triggered a giant atmospheric shock wave and tsunamis. The exact mechanism of this extraordinary eruptive event, its size and magnitude are not well understood yet. In this work, we analyze data from the nearest ground-based receivers of Global Navigation Satellite System to explore the ionospheric total electron content (TEC) response to this event. We show that the ionospheric response consists of a giant TEC increase followed by a strong long-lasting depletion. We observe that the explosive event of 15 January 2022 began at 04:05:54UT and consisted of at least five explosions. Based on the ionospheric TEC data, we estimate the energy released during the main major explosion to be between 9 and 37 Megatons in trinitrotoluene equivalent. This is the first detailed analysis of the eruption sequence scenario and the timeline from ionospheric TEC observations.

**Plain Language Summary** On 15 January 2022, the giant explosion of the Hunga Tonga-Hunga Ha'apai volcano shook the atmosphere of the Earth and generated a tsunami. The exact mechanism and timing of the eruption are not well understood yet, nor is the series of events that occurred directly following the first event. Many scientists are trying to understand the chronology of the eruption using different types of data. Here we investigate the signature of the eruption as recorded in Earth's ionosphere, the electrically conductive layer of the atmosphere from about 85 to 800 km of altitude. We observe variations in the total electron content (TEC) of the ionosphere using Global Navigation Satellite System receivers (commonly known as GPS receivers). Variations in the TEC through time and space are caused by sound waves from the eruption traveling through the ionosphere. We use these variations to constrain the timing of the eruptive events, identifying at least five major explosions during this eruption. In addition, we use the amplitude of TEC variations to estimate that the largest explosion released energy of about 9–37 Megaton in trinitrotoluene equivalent. This is the first detailed analysis of the eruption scenario and the timeline from ionospheric TEC observations.

## 1. Introduction

It is known that volcanic eruptions and explosions generate acoustic and gravity waves that reach the ionosphere and generate so-called co-volcanic ionospheric disturbances (CVIDs; e.g., Astafyeva, 2019; Meng et al., 2019). The ionospheric disturbances are usually registered about 10–45 min after the eruption onset and are observed directly above the volcano to as far away as 800–1,000 km (Dautermann et al., 2009; Heki, 2006; Manta et al., 2021; Nakashima et al., 2016; Shults et al., 2016). CVID often represent quasi-periodic variations of ionospheric electron density or of total electron content (TEC) with periods of 12–30 min (e.g., Dautermann et al., 2009; Shults et al., 2016). The apparent velocity of propagation can vary between 550 m/s and 1,100 km/s, which corresponds to gravito-acoustic, acoustic and shock-acoustic waves.

On 15 January 2022, a giant surtseyan volcanic explosion occurred at the uninhabited volcanic island Hunga Tonga-Hunga Ha'apai (HHTH) in South Pacific. The eruption caused the collapse of two-thirds of the volcanic edifice as reported from Sentinel 1 observations (<https://marine.copernicus.eu/news/satellites-observe-tsunami-triggered-tonga-volcano>), and triggered a tsunami. The interaction between the hot magma and sea water generated a large plume of ash and steam that reached as high as 33–35 km of altitude (e.g., Witze, 2022), and triggered giant atmospheric shock wave that propagated around the world several times (Duncombe, 2022). The

**Validation:** E. Astafyeva, B. Maletckii, T. D. Mikesell, M. Ravanelli, P. Coisson, L. Rolland

**Visualization:** E. Astafyeva, B. Maletckii, T. D. Mikesell

**Writing – original draft:** E. Astafyeva  
**Writing – review & editing:** E. Astafyeva, B. Maletckii, T. D. Mikesell, E. Munaibari, M. Ravanelli, P. Coisson, F. Manta, L. Rolland

eruption also generated large ionospheric disturbances that propagated around the world (Themens et al., 2022; Zhang et al., 2022).

The exact mechanism of the HTHH explosive eruption remains unknown, and the big scientific puzzle is complicated by the fact that the volcano is a submarine and ground-based instruments are not available nearby. Even the eruption onset time is still under debate. Observations from Himawari-8 satellite suggest that the eruption began sometime between 4:00 and 4:10UT (Gusman & Roger, 2022). The US Geological Survey (USGS), based on techniques calibrated for earthquakes, estimated that the eruption was equal to a M5.8 earthquake that began at 04:14:45UT (<https://earthquake.usgs.gov/earthquakes/eventpage/pt22015050/executive>). Poli and Shapiro (2022) based on analysis of long-period surface waves registered by seismic stations, calculated the onset at 04h16m00.07UT. Backprojection of surface pressure data in Tonga estimates the source time at 04:28 ± 02UT (Wright et al., 2022).

Here we study the ionospheric response to the HTHH explosion and, for the first time, we reconstruct the timeline of the HTHH eruption sequence fully based on ionospheric observations.

## 2. Data and Methods

Global Navigation Satellite Systems (GNSS) are nowadays widely used for ionosphere sounding. Phase measurements from dual-frequency GNSS receivers allow to estimate the ionospheric TEC, which is an integrated value equal to the number of electrons along a line-of-sight (LOS) between a satellite and a receiver:

$$\text{sTEC}_{\text{ph}} = \frac{1}{A} \cdot \frac{f_1^2 f_2^2}{f_1^2 - f_2^2} (L_1 \lambda_1 - L_2 \lambda_2) \quad (1)$$

where  $A = 40.308 \text{ m}^3/\text{s}^2$ ,  $L_1$  and  $L_2$  are phase measurements, and  $\lambda_1$  and  $\lambda_2$  are wavelengths at two GNSS frequencies. For the Global Positioning System (GPS) signals these are:  $\lambda_1 = 1,575.42$  and  $\lambda_2 = 1,227.60$  MHz. Most of GNSS (e.g., GPS, Galileo, BeiDou, QZSS) have fixed carrier frequencies. Whereas, in GLONASS each satellite has its own set of frequencies (e.g., Hofmann-Wellenhof et al., 2008; Shults et al., 2016).

In this study, the first data point is subtracted from the whole data series to remove an unknown bias that is always present in the phase measurements, that is, we are analyzing relative TEC. Further, in order to remove the strong TEC dependence on a LOS elevation angle, we convert the slant TEC to vertical TEC by using the single-layer mapping function (Schaer et al., 1995). The TEC data are displayed in TEC units (TECU), with 1 TECU equal to  $10^{16}$  electrons/ $\text{m}^2$ .

The spatial positions of ionospheric disturbances are calculated from so-called subionospheric points (SIPs), which are the projections of the intersection points between the LOS and the ionospheric thin shell at a fixed altitude that is often referred to as the altitude of detection  $H_{ion}$ . Here we take  $H_{ion} = 320$  km, which is close to the maximum ionization height  $H_mF2$  as derived from the nearest ionosonde station NIUE located at 190.07 E; 19.07 S (<https://lgdc.uml.edu/common/DIDBMonthListForYearAndStation?ursiCode=ND61R&year=2022>).

In this study, we analyze non-filtered TEC data, in order to keep the amplitude of the signal and temporal characteristics unchanged. This also enables to better investigate the link between the eruption features and the ionospheric response. We use 30-s data.

## 3. Results and Discussion

During the eruption, 15 ground-based GNSS-receivers were operational within ~2,000 km distance from the volcano (Figure 1a). Most of these receivers captured signals from GPS (code “G”), GLONASS (code “R”), Galileo (code “E”), Beidou (code “C”), SBAS (code “S”), and QZSS (code “J”) satellite constellations. The following satellites showed clear CVID signatures in the ionospheric TEC data: G10, G18, G23, G24, G32, R07, R20, R21, E03, E36, C01, C04, C23, C24, C25, C27, C28, S33 (Figure 1b). In addition, a few stations captured signals from J01, J02, J03, J04, and J07 satellites. Such an impressive number of observation points allowed us to analyze the CVID evolution with an unprecedented level of detail.

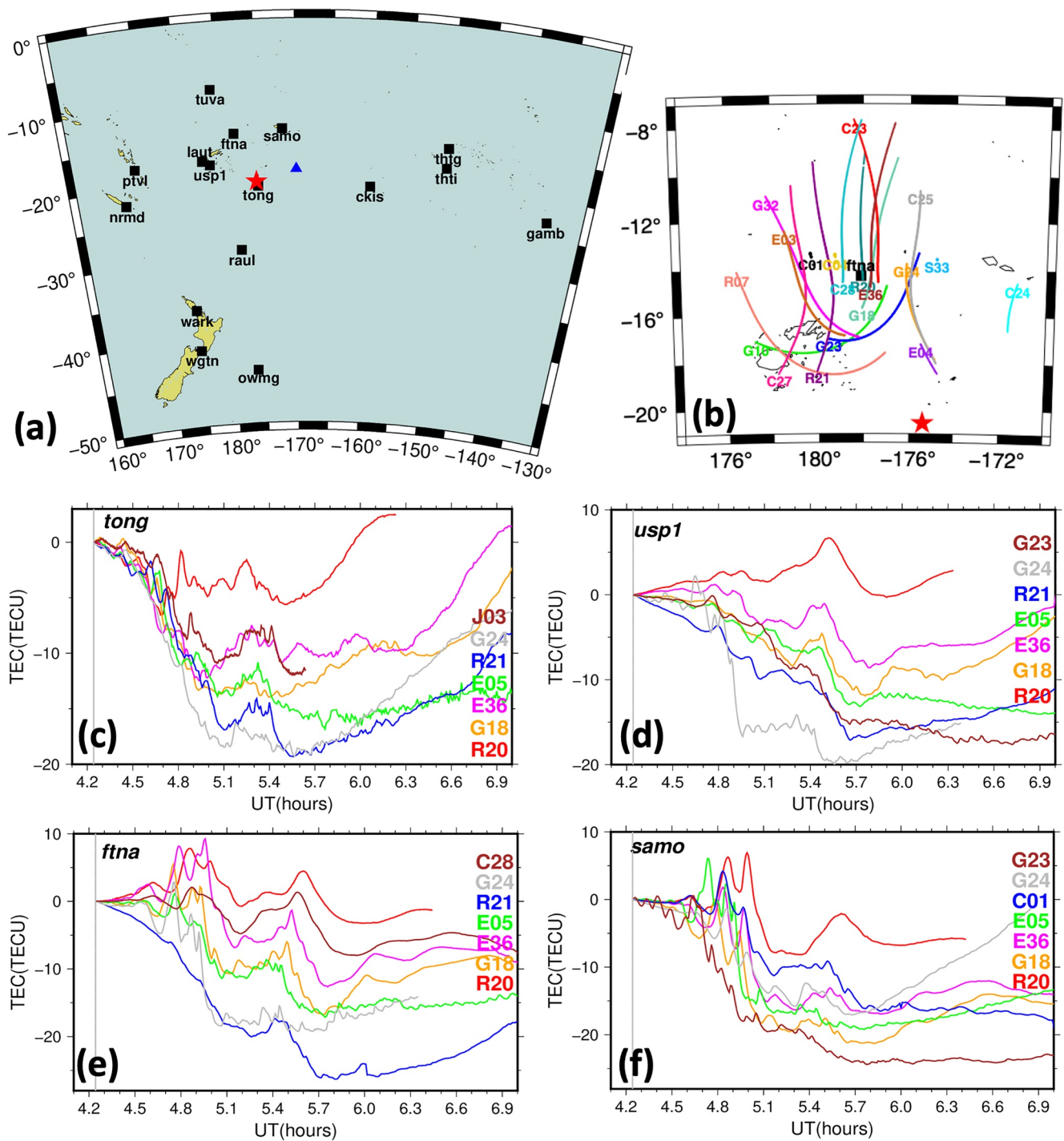


**Figure 1.** (a) The geometry of CVID observations by multiple Global Navigation Satellite Systems (GNSS). Black squares show the GNSS stations, the red star depicts the volcano (175.382 W; 20.53 S), blue triangle—the ionosonde station; (b) IPP trajectories for the station FTNA at the altitude  $H_{ion} = 320$  km, for the time period between 4:14 (the US Geological Survey eruption time onset) and 8UT. Satellite names are shown at the beginning of each IPP trajectory that corresponds to the eruption onset; (c–f) Ionospheric total electron content (TEC) variations registered by the four closest GNSS receivers: *tong* (c), *usp1* (d), *ftna* (e), and *samo* (f). Names of satellites are noted on the panels.

### 3.1. TEC Variations of Unprecedented Amplitude Due To Shock Waves

The ionospheric TEC data series registered near the volcano are presented in Figures 1c–1f. The first CVID signatures are visible at  $\sim 4.45$ UT, while several other large variations are seen at later times. Interestingly, these

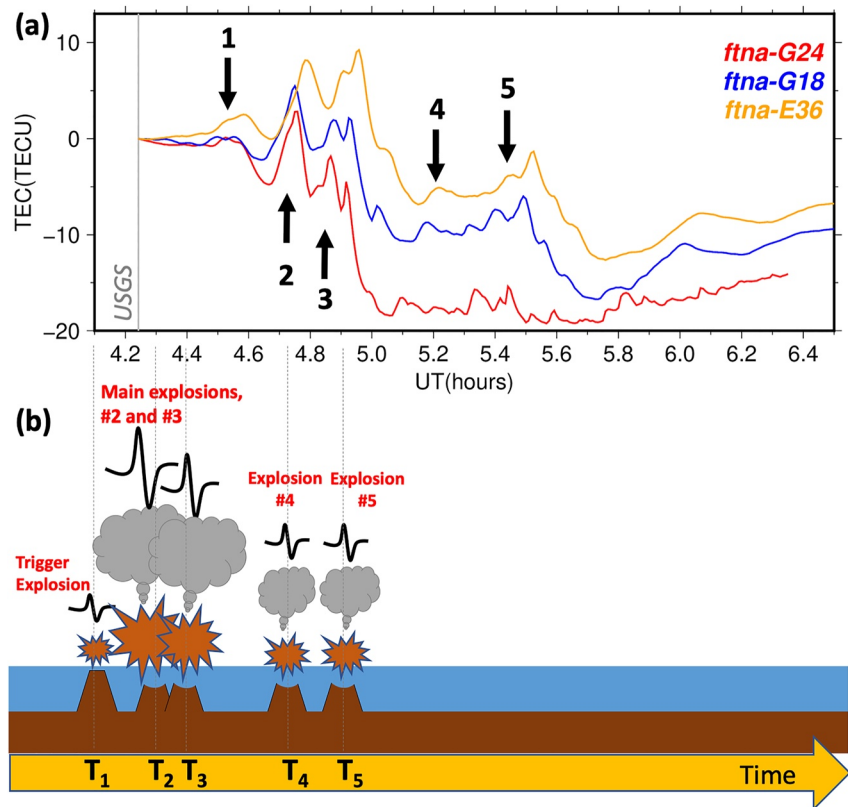


**Figure 2.** (a) Ionospheric disturbances corresponding to five explosions that most likely took place on 15 January 2022. Gray vertical line denotes the US Geological Survey onset time; (b) Suggested scenario and the timeline of the HTHH volcano explosions of 15 January 2022. Each explosion emits an acoustic pulse of different amplitude as illustrated. Vertical dotted lines correspond to the ionospherically determined onset times of the explosions.

TEC variations do not represent the “classic” quasi-periodic waveform observed in previous studies. These CVID are complex waveforms with a clear occurrence of N-waves with very sharp TEC increases, which is an indication of an acoustic or shock-acoustic wave source. Similar disturbances were observed following the giant M9 March 2011 Tohoku-Oki earthquake (e.g., Astafyeva et al., 2011; Liu et al., 2011).

The other remarkable observation is the amplitude of the TEC response to the HTHH eruption that reaches the extraordinary level of 5–8 TECU (Figures 1c–1f). Given the absolute background vertical TEC around the volcano varies from 18 to 23 TECU at the beginning of the eruption, we conclude that the CVID contribution to the background TEC is 21%–44%. This value is unprecedented with respect to previous studies that showed ~8% for eruptions with volcanic explosivity index (VEI) of 2%, and 15%–18% for VEI = 4 eruptions (Shults et al., 2016).

### 3.2. Multiple Volcanic Explosions Are Detected by the Ionosphere

We note that the TEC variations show multiple large peaks occurring between 4.45 and 5.6UT (Figures 1c–1f and 2a). We propose that these individual peaks represent individual explosions that occurred between 4 and 5UT (Figure 2b). The acoustic or shock-acoustic nature of the observed peaks can be confirmed from the N-type waveforms of the CVID and their apparent velocities (Figure S2 in Supporting Information S1). A similar complex TEC response was observed for the largest M9 earthquakes, driven by multiple rupturing segments of the megathrust fault: the 2011 Tohoku-Oki (Astafyeva, Rolland, et al., 2013) and the 2004 Sumatra earthquake (Heki et al., 2006).

The scenario of multiple explosions is in line with conclusions by Wright et al. (2022) made from the analysis of surface pressure data recorded at a station in Tonga, only 64 km away from the HTHH volcano. Wright et al. (2022) identified the first peak at 04:26UT and four other events at 04:36UT, 05:10UT, 05:51UT and 08:46UT.

**Table 1**

*Time Onsets of the Five HTHH Volcano Explosions as Estimated From the Ionosphere: By Using the Approximation of Spherical Wave at Constant Radial Velocity (Columns 4–5),  $Onset_{SPHER}$  and by Using the IonoSeis Software,  $Onset_{IonoSeis}$  (Column 6)*

#	Sub-event	CVID detection time (UT)	CVID radial velocity (m/s)	$Onset_{SPHER}$ (UT)	$Onset_{IonoSeis}$ (UT)	$Onset_{iono}$ (UT $\pm$ sec)
1	Trigger/initial event	04:20:00, 04:22:30	620	04:08:43	04:03:15	04:05:54 $\pm$ 169
2	Main explosion	04:25:30; 04:28:00	620	04:20:00	04:16:20	04:18:10 $\pm$ 110
3	Explosion 3	04:51:30; 04:53:00	510	04:28:05	04:24:45	04:26:25 $\pm$ 100
4	Explosion 4	05:05:30; 05:07:30	770	04:48:30	04:38:45	04:43:37 $\pm$ 292
5	Explosion 5	05:08:30; 05:15:30	550	04:55:21	04:54:45	04:54:27 $\pm$ 18

*Note.* The final ionospheric onset time was calculated by averaging the solutions in columns 5 and 6.

From the ionosphere, we can estimate the onset time by approximating CVID propagation as a spherical wave at a constant speed from a point source (Figure S1a in Supporting Information S1; Kiryushkin & Afraimovich, 2007). Shults et al. (2016) used such an approximation to locate the eruptive source position fully based on ionospheric data. Here, we modify the previous algorithm by fixing the source at the volcano position and by only varying the CVID radial speed in order to obtain the most probable onset time (Text S1 in Supporting Information S1). From TEC data, we select peaks with clear N-wave-like waveforms that could represent explosions. For each event, we determine the CVID arrival times at the moment when the TEC starts to increase suddenly (Figure S1b in Supporting Information S1), and the coordinates of the CVID detection (Tables S1–S5 in Supporting Information S1). From these data and by applying our method, we obtain the following onset times for the five sub-events/explosions (Figure 2a): event #1 that lead to the preparation of the big explosions and the caldera collapse, began at 04:08:43UT. The largest two explosions occurred at 04:20:00 UT and at 04:28:05UT, then smaller sub-events took place at 04:48:30UT (#4) and at 04:55:21 UT (#5) (Table 1). We note that other TEC peaks were analyzed but did not give a solution. We therefore consider that they are not of acoustic nature.

To confirm these proposed event times and multiple events scenario, we model individual explosive events using the IonoSeis package (Mikesell et al., 2019; Rolland et al., 2013). This model uses one-dimensional sound speed and density profiles (Figures 3a and 3b, respectively) based on the local date and time computed with NRLMSIS 2.0 (Emmert et al., 2020). The model uses a three-dimensional background electron density profile based on local date and time (IRI2016, Bilitza et al., 2017), as well as the local magnetic field inclination and declination (IGRF, Alken et al., 2021). IonoSeis propagates an acoustic N-shaped pulse through the atmosphere from the location of the volcano at the Earth's surface to the ionosphere (Dessa et al., 2005). The neutral atmospheric wave is coupled into the ionosphere model and the slant TEC variation between satellite-receiver is computed (Mikesell et al., 2019). More details about the parameters chosen in this study can be found in Text S2 in Supporting Information S1.

To reproduce the TEC series observed after the HTHH volcano explosion, five pulses of different amplitude were launched at different moments of time (Figure 3c). The modeling results confirm the occurrence of at least five explosions and also that events #2 and #3 were the largest. The simulations also provide us with another set of the onset times: the initial explosion (trigger) at 04:03:15UT, the main big explosion at 04:16:20UT, another big one at 04:24:45UT, and events #4 and #5 at 04:24:45UT and 05:02:15UT, respectively. The IonoSeis onsets are always 3.5–4.5 min ahead of those estimated by the spherical approximation method (Table 1), which can be explained by the difference in the approaches (constant velocity in the first method and a 1D velocity varying with altitude in the IonoSeis). Also, the spherical wave method is based on the manual determination of the arrival time, which can introduce additional inaccuracy. Knowing that IonoSeis tends to systematically delay the arrival of disturbance with respect to observations (Lee et al., 2018; Mikesell et al., 2019; Zedek et al., 2021), we provide the final ionospheric solution for the onset times by averaging the solutions by two ionospheric methods (Table 1). We obtain 04:05:54  $\pm$  169 s UT for the onset HTHH eruption trigger event and 04:18:10  $\pm$  110 UT for the main big explosion.

### 3.3. Explosion Energy Release as Estimated From the Ionosphere

From the ionospheric GNSS-derived TEC data it is possible to estimate the energy of the volcanic explosion (Dautermann et al., 2009; Heki, 2006). Heki (2006) suggested an empirical method based on analysis of CVID

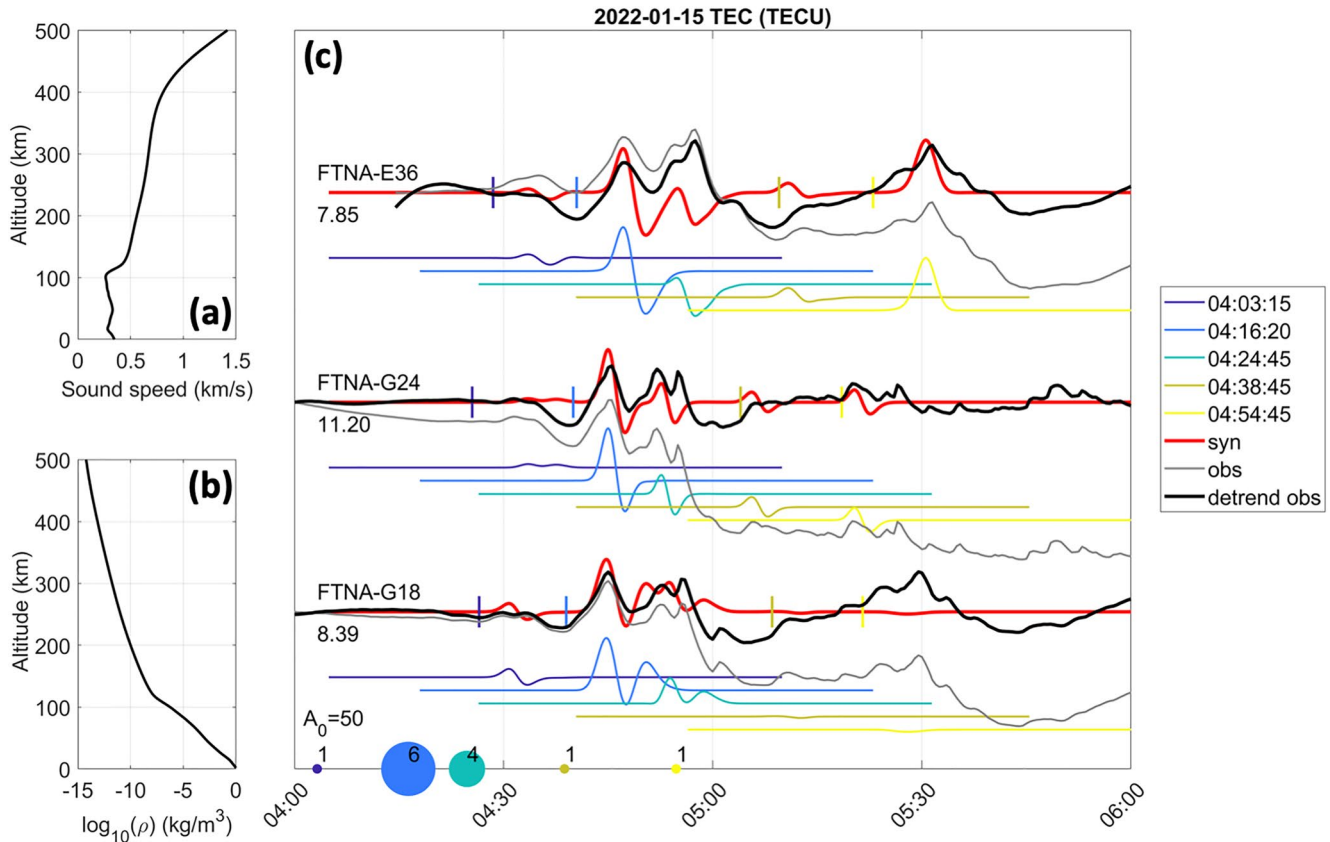


**Figure 3.** (a) Sound speed and (b) neutral density profiles used to model the total electron content (TEC) response by using IonoSeis software; (c) Comparison of slant TEC observations (gray and black curves) with IonoSeis simulations (red curves) for FTNA-E36, FTNA-G24, FTNA-G18 LOS. The black and gray slant TEC curves have been scaled by the coefficient indicated just above the receiver-satellite pair name. Thin colored curves show different pulses launched at different moments of time as shown on the legend on the right. The dots on the bottom  $x$ -axis indicate relative size of source based on a scalar amplitude factor. The numbers are relative to the first event, which has amplitude 1.

amplitudes with respect to the background TEC and comparison of the TEC response to Wyoming mine blasts of known explosive power by Calais et al. (1998). In that latter case, the explosion power of 1.5 kiloton in trinitrotoluene (TNT) equivalent generated TEC disturbance with the maximum amplitude of 0.03 TECU on the background absolute VTEC of 10.6 TECU. By using this method, Heki (2006) estimated the energy of the VEI = 2 Asama volcano explosion as of  $\sim 4 \times 10^4$  t TNT or  $2 \times 10^{14}$  J. However, it is important to note that besides the background TEC, other two factors affect the amplitude of CVID: the magnetic field configuration and the angle between the LOS and the disturbance wavefront (Bagiya et al., 2019; Kakinami et al., 2013; Otsuka et al., 2006; Rolland et al., 2013). Therefore, these parameters should be taken into account when comparing the disturbance amplitudes on the day of the Wyoming blast and the HTHH explosion.

In our case, multiple LOS on the north-west and north-east from the volcano detect CVID with similar amplitudes of 5–8 TECU, therefore, we conclude that the impact of the LOS-wavefront intersection is less important for such a huge event. Therefore, the rough estimation of the energy release is estimated by taking the maximum CVID amplitudes 5 and 8 TECU (at *samo-E03*, *usp1-G24*, *ftna-G24*, *ftna-E36*, *samo-R20*), and the background TEC (between 18 and 23 TECU). Knowing that the wave energy scales with the square of the amplitude, we estimate that the HTHH explosion is about 5,900 and 24,700 times more powerful than the mine blasts studied by Calais et al. (1998). Therefore, the HTHH explosion power is between  $\sim 9$  and 37 megaton (Mt) in TNT equivalent, or between  $\sim 3.7 \times 10^{16}$  and  $1.5 \times 10^{17}$  J. This value is in agreement with estimations from other instruments and methods between 4 and 18 Mt of TNT (Garvin, 2022), and it is of the order of the 1,883 Krakatoa volcano explosion, for which the acoustic energy was estimated as high as  $8.6 \times 10^{16}$  J (Woulff & McGetchin, 1976). The fact that the HTHH explosion generated a huge Lamb wave that traveled around the world at least 3 times (e.g., Zhang et al., 2022) is additional indication of the similar energy release with the Krakatoa explosion.

### 3.4. The Giant and Long-Lasting Ionospheric Hole

In Figures 1c–1f, we notice an abrupt decrease in TEC starting from  $\sim 4.7$ UT. This decrease is clearly observed by comparing the event data series to four quiet days preceding the eruption (10–13 January 2022) and the day after (Figure 4). Although we see day-to-day variations, the depletion is only present on 15 January. This ionospheric depletion (“hole”) resembles TEC response to the Tohoku-Oki earthquake and several other large earthquakes (e.g., Astafyeva, Shalimov, et al., 2013; Kakinami et al., 2012). Astafyeva, Shalimov, et al. (2013) demonstrated that the magnitude and the duration of the depletion scales with the magnitude of an earthquake

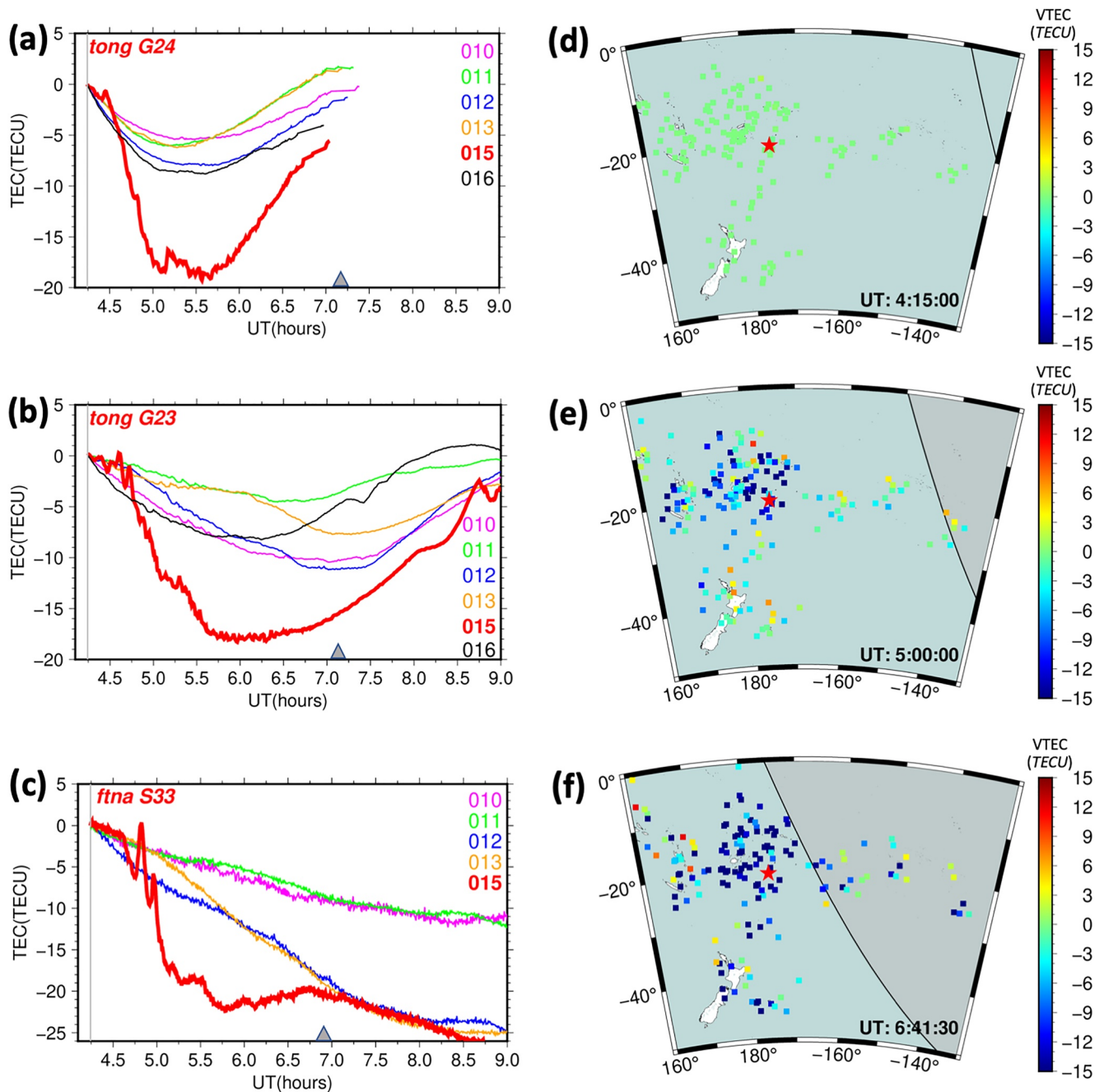


**Figure 4.** (a–c) Ionospheric depletion as seen on the eruption day (red curve, 015) with respect to four quiet days before (010, 011, 012, 013) and the day after the eruption (016) as recorded by *tong* station and *G24* satellite (a), *tong G23* (b), and *ftna S33* (c). Gray triangles depict the approximate time of the solar terminator; (d–f) total electron content snapshots plotted by using data of all satellites and all stations shown in Figures 1a and 1b: (d) close to the eruption onset at 04:15UT; (e–f) during the depletion observations at 05:00UT and 06:41UT.

and explained the hole as the rarefaction phase of the shock-acoustic wave. For the 2011 Tohoku-Oki earthquake, the depletion lasted 30–50 min and the TEC decreased by  $-5$  to  $-6$  TECU with respect to the before-earthquake level (Astafyeva, Shalimov, et al., 2013; Astafyeva, Rolland, et al., 2013). In the case of the HTHH event, the depletion of the amplitude of  $-13$  to  $18$  TECU lasted for at least 1.5–2 hr (Figure 4), which is unprecedented, both in magnitude and duration. This could be explained, first of all, by the fact that eruptive explosions should generate stronger shock waves than earthquakes because the source is located at shallow depth (about 200 m) under water but not underground. The giant shock wave would cause large-amplitude and long-lasting rarefaction phase. Similarly, Aa et al. (2022) suggested that the depletion was composed of cascading TEC decreases due to different acoustic wave impulses.

Second, it is possible that the HTHH ionospheric depletion was reinforced by a geomagnetic storm that began several hours before the eruption, and was in an early recovery phase at the time of the CVID observations. While the storm was moderate (minimum Dst excursion of  $-100$  nT, World Data Center for Geomagnetism et al., 2015), the storm-time composition changes were significant, as the data of the Global Ultraviolet Imager (GUVI) onboard the Thermosphere, Ionosphere, Mesosphere Energetics and Dynamics (TIMED) satellite (<http://guvitimed.jhuapl.edu/>, Christensen et al., 2003) show (Figure S3 in Supporting Information S1). The  $O/N_2$  ratio was reduced above the area of the CVID observations, which means decreased ionization (e.g., Prölss, 1976).

Third, unlike the Tohoku-Oki earthquake that occurred in the local afternoon, the HTHH depletion developed during local evening hours, which undoubtedly also have played a role in the retarded recovery from the hole because of the decreased evening ionization level.

The extremely low local ionization level due to the depletion made it difficult to clearly detect and to analyze one later eruption that took place around 8:30UT (Figure S4 in Supporting Information S1; Wright et al., 2022).

#### 4. Conclusions

The extraordinary Hunga Tonga-Hunga Ha'apai volcano eruption and related explosive events generated quite significant and long-lasting effects in the ionosphere. Shortly after the eruption onset, GNSS-receivers around the volcano area showed TEC variations with several distinct peaks that correspond, most likely, to a trigger event (the initial explosion) at  $04:05:54 \pm 169$  s UT and four other explosions that occurred between 4:18 and 4:54UT on 15 January 2022.

The second and the most powerful explosion occurred at 04:18:10UT. Based on the CVID amplitudes and the background TEC value, we estimate that this major explosion released energy between 9 and 37 Megaton in TNT equivalent, that is comparable to the 1883 Krakatoa event.

The large TEC increase was followed by major depletion in the ionosphere in the vicinity of the volcano. The TEC dropped by  $-13$  to  $-18$  TECU below the quiet TEC values, and the depletion lasted for at least 1.5–2 hr, which is unprecedented. The depletion was primarily caused by the giant shock waves.

We demonstrate that numerous ionospheric sounding points in the vicinity of the volcano can help to decipher the eruption scenario and chronology. This is the first study of the kind.

#### Data Availability Statement

All GNSS data are available from the CDDIS archives [https://cddis.nasa.gov/Data\\_and\\_Derived\\_Products/GNSS/daily\\_30second\\_data.html](https://cddis.nasa.gov/Data_and_Derived_Products/GNSS/daily_30second_data.html) and data of RAUL station are from the Geological hazard information for New Zealand (GeoNet) database via <https://data.geonet.org.nz/gnss/rinex/2022/015/>. The thermospheric  $O/N_2$  composition data are available from: <http://guvitimed.jhuapl.edu/guvi-gallery13on2>. The TEC estimation “tec-suite” codes are accessible from <https://tec-suite.readthedocs.io/en/latest/installation.html>. The GMT6.0 software is available at <https://www.generic-mapping-tools.org/download/>.

### Acknowledgments

This work was supported by the French Space Agency (CNES), projects “Real-Detect” (EA, BM) and “UV-TECGEOX” (LR, EM). LR, EM and TDM acknowledge the support of the French National Agency of Research (ANR), project ITEC (Grant ANR-19-CE04-0003), and project Université Côte d’Azur Investissement d’Avenir IDEX. MB, EM and MR thank the CNES for the PhD and PostDoctoral Fellowships. We thank I. Zhivetiev for the “tec-suite” codes. Figures were done by using the GMT6.0 software (Wessel et al., 2019).

### References

- Aa, E., Zhang, S.-R., Erickson, P. J., Vierinen, J., Coster, A. J., Goncharenko, L. P., et al. (2022). Significant equatorial plasma bubbles and global ionospheric disturbances after the 2022 Tonga volcano eruption. *Earth and Space Science Open Archive*. <https://doi.org/10.1002/essoar.10510637.1>
- Alken, P., Thébault, E., Beggan, C. D., Amit, H., Aubert, J., Baerenzung, J., et al. (2021). International geomagnetic reference field: The thirteenth generation. *Earth, Planets and Space*, 73, 49. <https://doi.org/10.1186/s40623-020-01288-x>
- Astafyeva, E. (2019). Ionospheric detection of natural hazards. *Reviews of Geophysics*, 57(4), 1265–1288. <https://doi.org/10.1029/2019RG000668>
- Astafyeva, E., Lognonné, P., & Rolland, L. (2011). First ionosphere images for the seismic slip on the example of the Tohoku-Oki earthquake. *Geophysical Research Letters*, 38(22), L22104. <https://doi.org/10.1029/2011GL049623>
- Astafyeva, E., Rolland, L., Lognonné, P., Khelifi, K., & Yahagi, T. (2013). Parameters of seismic source as deduced from 1 Hz ionospheric GPS data: Case-study of the 2011 Tohoku-Oki event. *Journal of Geophysical Research*, 118(9), 5942–5950. <https://doi.org/10.1002/jgra.50556>
- Astafyeva, E., Shalimov, S., Olshanskaya, E., & Lognonné, P. (2013). Ionospheric response to earthquakes of different magnitudes: Larger quakes perturb the ionosphere stronger and longer. *Geophysical Research Letters*, 40(9), 1675–1681. <https://doi.org/10.1002/grl.50398>
- Bagiya, M. S., Sunil, A. S., Rolland, L., Nayak, S., Ponraj, M., Thomas, D., & Ramesh, D. S. (2019). Mapping the impact of non-tectonic forcing mechanisms on GNSS measured coseismic ionospheric perturbations. *Scientific Reports*, 9(1), 18640. <https://doi.org/10.1038/s41598-019-54354-0>
- Bilitza, D., Altadill, D., Truhlik, V., Shubin, V., Galkin, I., Reinisch, B., & Huang, X. (2017). International Reference Ionosphere 2016: From ionospheric climate to real-time weather predictions. *Space Weather*, 15(2), 418–429. <https://doi.org/10.1002/2016SW001593>
- Calais, E., Minster, J. B., Hofton, M. A., & Hedlin, H. (1998). Ionospheric signature of surface mine blasts from Global Positioning System measurements. *Geophysical Journal International*, 132(1), 191–202. <https://doi.org/10.1046/j.1365-246x.1998.00438.x>
- Christensen, A. B., Paxton, L. J., Avery, S., Craven, J., Crowley, G., Humm, D. C., et al. (2003). Initial observations with the Global Ultraviolet Imager (GUVI) on the NASA TIMED satellite mission. *Journal of Geophysical Research*, 108(A12), 1451. <https://doi.org/10.1029/2003JA009918>
- Dautermann, T., Calais, E., & Mattioli, G. S. (2009). Global positioning system detection and energy estimation of the ionospheric wave caused by the 13 July 2003 explosion of the Soufrière Hills volcano, Montserrat. *Journal of Geophysical Research*, 114(B2), B02202. <https://doi.org/10.1029/2008JB005722>
- Dessa, J. X., Virieux, J., & Lambotte, S. (2005). Infrasound modeling in a spherical heterogeneous atmosphere. *Geophysical Research Letters*, 32(12), 1–5. <https://doi.org/10.1029/2005GL022867>
- Duncombe, J. (2022). The surprising reach of Tonga’s giant atmospheric waves. *EOS*, 103. <https://doi.org/10.1029/2022EO20050>
- Emmert, J. T., Drob, D. P., Picone, J. M., Siskind, D. E., Jones, M., Jr., Mlynczak, M. G., et al. (2020). Nrlmsis 2.0: A whole-atmosphere empirical model of temperature and neutral species densities. *Earth and Space Science*, 7(3), e2020EA001321. <https://doi.org/10.1029/2020EA001321>
- Garvin, J. (2022). *Dramatic changes at Hunga Tonga-Hunga Ha’apai*. Retrieved from <https://earthobservatory.nasa.gov/images/149367/dramatic-changes-at-hungatonga-hunga-haapai>
- Gusman, A. R., & Roger, J. (2022). *Hunga Tonga—Hunga Ha’apai volcano-induced sea level oscillations and tsunami simulations*. GNS Science Webpage. <https://doi.org/10.21420/DYKJ-RK41>
- Heki, K. (2006). Explosion energy of the 2004 eruption of the Asama Volcano, central Japan, inferred from ionospheric disturbances. *Geophysical Research Letters*, 33(14), L14303. <https://doi.org/10.1029/2006GL026249>
- Heki, K., Otsuka, Y., Choosakul, N., Hemmakorn, N., Komolmis, T., & Maruyama, T. (2006). Detection of ruptures of Andaman fault segments in the 2004 Great Sumatra Earthquake with coseismic ionospheric disturbances. *Journal of Geophysical Research*, 111(B9), B09313. <https://doi.org/10.1029/2005JB004202>
- Hofmann-Wellenhof, B., Lichtenegger, H., & Wasle, E. (2008). *GNSS-global navigation satellite systems*. Springer. <https://doi.org/10.1007/978-3-211-73017-1>
- Kakinami, Y., Kamogawa, M., Tanioka, Y., Watanabe, S., Gusman, A. R., Liu, J. Y., et al. (2012). Tsunamigenic ionospheric hole. *Geophysical Research Letters*, 39(13), L00G27. <https://doi.org/10.1029/2011GL050159>
- Kakinami, Y., Kamogawa, M., Watanabe, S., Odaka, M., Mogi, T., Liu, J. Y., et al. (2013). Ionospheric ripples excited by superimposed wave fronts associated with Rayleigh waves in the thermosphere. *Journal of Geophysical Research*, 118(2), 905–911. <https://doi.org/10.1002/jgra.50099>
- Kiryushkin, V. V., & Afraimovich, E. L. (2007). Determining the parameters of ionospheric perturbation caused by earthquakes using the quasi-optimum algorithm of spatiotemporal processing of TEC measurements. *Earth Planets and Space*, 59(4), 267–278. <https://doi.org/10.1186/bf03353104>
- Lee, R. F., Rolland, L. M., & Mikesell, T. D. (2018). Seismo-ionospheric observations, modeling, and backprojection of the 2016 Kaikōura earthquake. *Bulletin of the Seismological Society of America*, 108(3B), 1794–1806. <https://doi.org/10.1785/0120170299>
- Liu, J. Y., Chen, C. H., Lin, C. H., Tsai, H. F., Chen, C. H., & Kamogawa, M. (2011). Ionospheric disturbances triggered by the 11 March 2011 M9.0 Tohoku earthquake. *Journal of Geophysical Research*, 116(A6), A06319. <https://doi.org/10.1029/2011JA016761>
- Manta, F., Occhipinti, G., Hill, E., Perttu, A., & Taisne, B. (2021). Correlation between GNSS-TEC and eruption magnitude supports the use of ionospheric sensing to complement volcanic hazard assessment. *Journal of Geophysical Research: Solid Earth*, 126(2). <https://doi.org/10.1029/2020JB020726>
- Meng, X., Vergados, P., Komjathy, A., & Verkhoglyadova, O. (2019). Upper atmospheric responses to surface disturbances: An observational perspective. *Radio Science*, 54(11), 1076–1098. <https://doi.org/10.1029/2019RS006858>
- Mikesell, T. D., Rolland, L. M., Lee, R. F., Zedek, F., Coisson, P., & Dessa, J.-X. (2019). IonoSeis: A package to model coseismic ionospheric disturbances. *Atmosphere*, 10(8), 443. <https://doi.org/10.3390/atmos10080443>
- Nakashima, Y., Heki, K., Takeo, A., Cahyadi, M. N., Aditiya, A., & Yoshizawa, K. (2016). Atmospheric resonant oscillations by the 2014 eruption of the Kelud volcano, Indonesia, observed with the ionospheric total electron contents and seismic signals. *Earth and Planetary Science Letters*, 434, 112–116. <https://doi.org/10.1016/j.epsl.2015.11.029>
- Otsuka, Y., Kotake, N., Tsugawa, T., Shiokawa, K., Ogawa, T., Effendy, et al. (2006). GPS detection of total electron content variations over Indonesia and Thailand following the 26 December 2004 earthquake. *Earth Planets and Space*, 58(2), 159–165. <https://doi.org/10.1186/BF03353373>
- Poli, P., & Shapiro, M. (2022). Rapid characterization of large volcanic eruptions: Measuring the impulse of the Hunga Tonga explosion from teleseismic waves. *Geophysical Research Letters*, 49(8), e2022GL098123. <https://doi.org/10.1029/2022GL098123>
- Pröls, G. W. (1976). On explaining the negative phase of ionospheric storms. *Planetary and Space Science*, 24(6), 607–609. [https://doi.org/10.1016/0032-0633\(76\)90140-9](https://doi.org/10.1016/0032-0633(76)90140-9)

- Rolland, L. M., Vergnolle, M., Nocquet, J.-M., Sladen, A., Dessa, J.-X., Tavakoli, F., et al. (2013). Discriminating the tectonic and non-tectonic contributions in the ionospheric signature of the 2011, Mw7.1, dip-slip Van earthquake, Eastern Turkey. *Geophysical Research Letters*, *40*(11), 2518–2522. <https://doi.org/10.1002/grl.50544>
- Schaer, S., Beutler, G., Mervart, L., & Rothacher, M. (1995). Global and regional ionosphere models using the GPS double difference phase observable. In *Proceedings of the 1995 IGS Workshop, Potsdam, Germany, May 15–17, 1995*. Retrieved from <https://mediatum.ub.tum.de/doc/1365730/137709.pdf>
- Shults, K., Astafyeva, E., & Adourian, S. (2016). Ionospheric detection and localization of volcano eruptions on the example of the April 2015 Calbuco events. *Journal of Geophysical Research: Space Physics*, *121*(10), 10303–10315. <https://doi.org/10.1002/2016JA023382>
- Themens, D. R., Watson, C., Žagar, N., Vasylykevych, S., Elvidge, S., McCaffrey, A., et al. (2022). Global propagation of ionospheric disturbances associated with the 2022 Tonga Volcanic Eruption. *Geophysical Research Letters*, *49*(7), e2022GL098158. <https://doi.org/10.1029/2022GL098158>
- Wessel, P., Luis, J. F., Uieda, L., Scharroo, R., Wobbe, F., Smith, W. H. F., & Tian, D. (2019). The generic mapping tools version 6. *Geochemistry, Geophysics, Geosystems*, *20*(11), 5556–5564. <https://doi.org/10.1029/2019GC00851>
- Witze, A. (2022). Why the Tongan volcanic eruption was so shocking. *Nature*, *602*, 376–378. <https://doi.org/10.1038/d41586-022-00394-y>
- World Data Center for Geomagnetism, Kyoto, M., Nose, Iyemori, T., Sugiura, M., & Kamei, T. (2015). *Geomagnetic Dst index*. <https://doi.org/10.17593/14515-74000>
- Woulff, G., & McGetchin, T. R. (1976). Acoustic noise from volcanoes—Theory and experiment. *Geophysical Journal of the Royal Astronomical Society*, *45*(4), 601–616. <https://doi.org/10.1111/j.1365-246x.1958.tb05346.x>
- Wright, C. J., Hindley, N., Alexander, M. J., Barlow, M., Hoffmann, L., Mitchell, C., et al. (2022). Tonga eruption triggered waves propagating globally from surface to edge of space. *Earth and Space Science Open Archive*. <https://doi.org/10.1002/essoar.10510674.1>
- Zedek, F., Rolland, L. M., Mikesell, T. D., Sladen, A., Delouis, B., Twardzik, C., & Coïsson, P. (2021). Locating surface deformation induced by earthquakes using GPS, GLONASS and Galileo ionospheric sounding from a single station. *Advances in Space Research*, *68*(8), 3403–3416. <https://doi.org/10.1016/j.asr.2021.06.011>
- Zhang, S.-R., Vierinen, J., Aa, E., Goncharenko, L. P., Erickson, P. J., Rideout, W., et al. (2022). 2022 Tonga volcanic eruption induced global propagation of ionospheric disturbances via Lamb waves. *Frontiers in Astronomy and Space Sciences*, *9*, 871275. <https://doi.org/10.3389/fspas.2022.871275>

## Reference From the Supporting Information

- Fuller-Rowell, T. J., Codrescu, M. V., Moffett, R. J., & Quegan, S. (1994). Response of the thermosphere and ionosphere to geomagnetic storms. *Journal of Geophysical Research*, *99*(A3), 3893–3914. <https://doi.org/10.1029/93JA02015>